



OPEN

New identification and significance of Early Cretaceous mafic rocks in the interior South China Block

Hui-Min Su¹, Shao-Yong Jiang^{1✉}, Jia-Bin Shao¹, Dong-Yang Zhang¹, Xiang-Ke Wu² & Xi-Qiang Huang²

Early Cretaceous mafic rocks are first reported in the northern Guangxi region from the western Qin-Hang belt in the interior South China Block. A systematic investigation of zircon U–Pb dating, whole-rock geochemistry, Sm–Nd isotopes and zircon Hf–O isotopes for these mafic rocks reveals their petrogenesis and the mantle composition as well as a new window to reconstruct lithospheric evolution in interior South China Block during Late Mesozoic. Zircon U–Pb dating yielded ages of 131 ± 2 Ma to 136 ± 2 Ma for diabase and gabbro from Baotan area, indicating the first data for Early Cretaceous mafic magmatism in the western Qin-Hang belt. These mafic rocks show calc-alkaline compositions, arc-like trace element distribution patterns, low zircon $\epsilon_{\text{Hf}}(t)$ of -9.45 to -6.17 and high $\delta^{18}\text{O}$ values of $+5.72$ to $+8.09\text{‰}$, as well as low whole-rock $\epsilon_{\text{Nd}}(t)$ values of -14.27 to -9.53 . These data suggest that the studied mafic rocks are derived from an ancient lithospheric mantle source that was metasomatized during Neoproterozoic subduction. Thus, the occurrence of these mafic rocks indicates a reactivation of Neoproterozoic subducted materials during an extension setting at Late Mesozoic in the western Qin-Hang belt, an old suture zone that amalgamates the Yangtze and Cathaysia blocks.

South China Block (SCB) can be divided into the Yangtze Block (YB) and Cathaysia Block (CB) separated by the Qin-Hang belt (Fig. 1a,b), which was suggested as a Paleo-subduction zone in the Late Mesoproterozoic to Early Neoproterozoic, and afterwards the SCB underwent multiple episodes of intracontinental reworking¹. In the CB, occurrences of Late Mesozoic mafic rocks and basalts are widely reported in particular in the eastern part of CB which are thought to be related to paleo-Pacific plate subduction². In the Qin-Hang belt (QHB), occurrence of Early-Middle Jurassic mafic intrusive and volcanic rocks are reported only in the Nanling Range and eastern QHB, such as the Daoxian and Ningyuan basalts from southern Hunan (150–154 Ma and 170–174 Ma)³, and Antang basalts from central Jiangxi (168 Ma)⁴, however, up to now, no Late Mesozoic mafic rocks have been reported in the western QHB which locates further interior in the SCB. Therefore, it is still highly debatable whether or not the paleo-Pacific plate subduction can reach up to the interior SCB as far as the YB, and if so, what is the role of the paleo-suture zone of Neoproterozoic that amalgamates the two blocks of YB and CB. In this paper, we report our recent investigations that identified several Late Mesozoic mafic intrusions (gabbro and diabase) from the Baotan area of the northern Guangxi region which located along the western QHB in the YB side just next to the western interior CB (Fig. 1b,c). Our new data suggest that these mafic rocks are generated via reactivation of paleo-subduction derived materials during an extension setting at Late Mesozoic in the western QHB, an old suture zone that amalgamates the Yangtze and Cathaysia blocks.

Geology of the studied region and occurrence of mafic rocks

In the northern Guangxi region of the western QHB occur mainly of Precambrian (meta-) sedimentary strata of Sibao Group and Danzhou Group and igneous rocks of early and middle Neoproterozoic, including voluminous granitoids and mafic–ultramafic rocks (Fig. 1c). The majority of the mafic–ultramafic intrusions are distributed in the Baotan, Sanfang and Yuanbaoshan areas (Fig. 1c) with more than 300 outcrops and a total exposed area of ca. 140 km² that are dated at 812–855 Ma^{7–9}.

Both gabbro and diabase occur as irregular shaped intrusions in the Mandong area that intruded into Neoproterozoic metasedimentary strata (Supplementary Fig. S1a,b). The gabbro is also in fault contact with the Neoproterozoic mineralized pyroxenite (Supplementary Fig. S1c). The gabbro in Gaobang and diabase in Wende

¹State Key Laboratory of Geological Processes and Mineral Resources, Collaborative Innovation Center for Exploration of Strategic Mineral Resources, School of Earth Resources, China University of Geosciences, Wuhan 430074, China. ²Guangxi Institute of Geological Survey, Guangxi Bureau of Geology and Mineral Prospecting and Exploitation, Nanning 530023, China. ✉email: shyjiang@cug.edu.cn

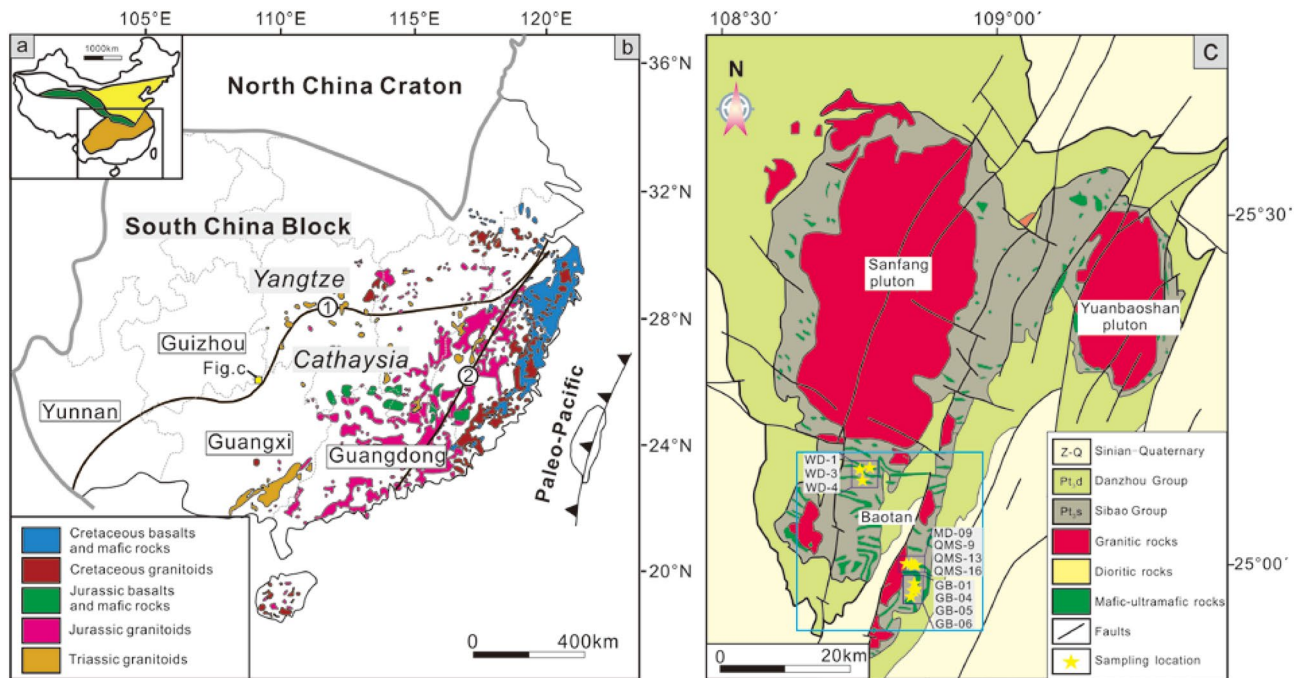


Figure 1. (a) Major tectonic units of China (modified from Ref.⁵). (b) Simplified map showing the distributions of the Mesozoic magmatism in SCB (modified from Ref.⁵). ① Qinzhou-Hangzhou belt, ② Zhenghe-Dapu fault zone. (c) Geological map of the northern Guangxi region showing the distribution of granites and mafic-ultramafic rocks with sample locations (modified from Ref.⁶).

occur as stock and small intrusion that intruded into the Sibao Group (Supplementary Fig. S1d). Different from the widespread Neoproterozoic mafic rocks that have been subjected to variable degrees of alteration and/or mineralization in this region^{10,11}, the mafic rock samples collected in this study are relatively fresh and suffered only very slightly alteration.

Mandong and Gaobang gabbros exhibit typical gabbro textures, mainly composed of 40% clinopyroxene, 50% plagioclase, 5% amphibole and 5% quartz (Supplementary Fig. S2a,b). Accessory phases mainly include apatite, titanite, and rutile. Mandong and Wende diabases are of porphyritic textures with phenocrysts of clinopyroxene, plagioclase and rare amphibole (Supplementary Fig. S2c,d). The matrix is microgranular and comprises dominant plagioclase, biotite, clinopyroxene, and minor K-feldspar and quartz. Minor clinopyroxene phenocrysts were locally replaced by an alteration assemblage of biotite (Supplementary Fig. S2d).

Results

Zircon U–Pb dating. Cathodoluminescence (CL) images of representative zircon grains from selected mafic rock samples in the northern Guangxi region are shown in Fig. 2. The Secondary ionization mass spectrometry (SIMS) and laser ablation inductively coupled plasma-mass spectrometry (LA-ICP-MS) zircon U–Pb dating results are listed in Supplementary Table S1 and shown in Fig. 2.

Fifteen analyses were carried out from Mandong (MD-15) and Wende (WD-1) diabase, respectively. An analysis point 9 on a whitish zircon from the sample MD-15 gives a youngest $^{206}\text{Pb}/^{238}\text{U}$ age of 81 ± 1 Ma, which may be caused by lead loss. Thus, this analysis was excluded from the final age calculation. Zircons from the Mandong diabase yield a weighted mean $^{206}\text{Pb}/^{238}\text{U}$ age of 131 ± 2 Ma (MSWD = 1.5, $n = 9$), those from the Wende diabase show a weighted mean $^{206}\text{Pb}/^{238}\text{U}$ age of 131 ± 2 Ma (MSWD = 1.7, $n = 11$). Older zircons (156–2246 Ma) (Fig. 2a,c) are also determined in both samples which indicate a detrital origin that originated from assimilation of wall rocks during magma ascent or inherited grains from the magma source region^{12,13}. The Gaobang gabbro also show a wide range of zircon ages with nine youngest analyses forming a tight cluster and give a weighted mean $^{206}\text{Pb}/^{238}\text{U}$ age of 136 ± 2 Ma (MSWD = 2.7) (Fig. 2e). Therefore, the age data from the above studied samples indicate an early Cretaceous age for the mafic magmatism in northern Guangxi, which is the first report of Late Mesozoic mafic rocks in this region.

Major and trace element concentrations. The studied mafic rocks are characterized by elevated SiO_2 (50.86–56.09 wt%), unusually low TiO_2 (0.33–0.65 wt%) and moderate CaO (6.16–9.46 wt%) and Al_2O_3 contents (12.34–17.20 wt%). In addition, these samples show relatively high FeO^T (11.10–15.48 wt%) and variable MgO (4.99–9.81 wt%) concentrations with $\text{Mg}^\#$ value of 50–68 (Supplementary Table S2). Plot of $\text{Na}_2\text{O} + \text{K}_2\text{O}$ vs. SiO_2 shows that these samples belong to subalkalic gabbro and gabbroic-diorite (Fig. 3a). On the FeO^T/MgO versus SiO_2 diagram (Fig. 3b), all samples plot in the calc-alkaline field.

These mafic rocks have lower total rare earth element (REE) contents (49.0–96.1 ppm) (Fig. 4a–c). They display broadly similar REE pattern showing an enrichment in light rare earth elements (LREE) and flat heavy

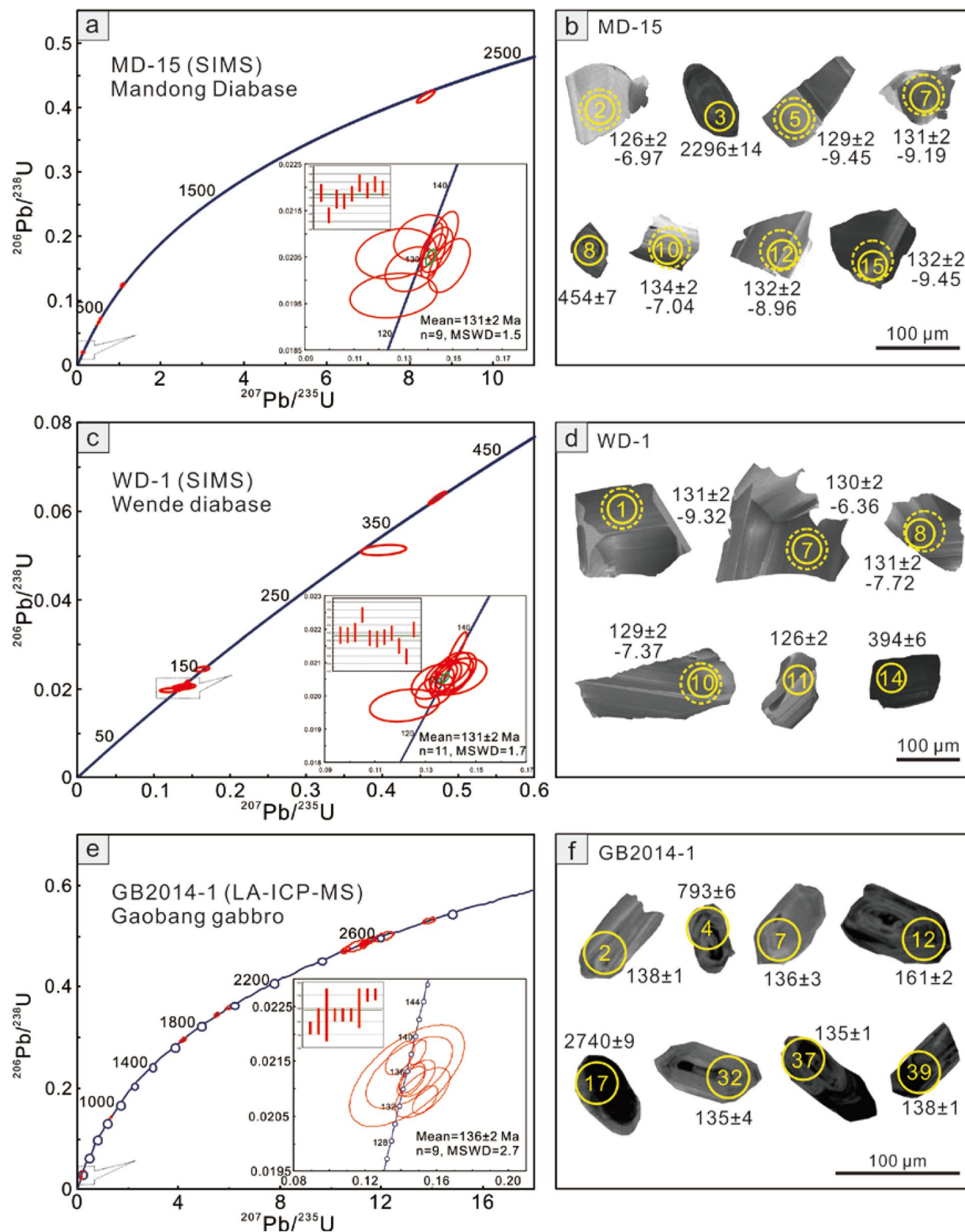


Figure 2. SIMS and LA-ICP-MS zircon U–Pb concordia diagrams for the studied mafic rocks (a,c,e) and cathodoluminescence (CL) images of the representative zircon grains for the studied mafic rocks (b,d,f). Solid circles represent the laser spots for U–Pb analysis, dashed spots for Hf isotope analysis.

rare earth elements (HREE) pattern with $(\text{La}/\text{Yb})_n$ ratios of 3.3 to 5.7 and $(\text{Gd}/\text{Yb})_n$ ratios of 1.1–1.4 (Fig. 4a–c; Supplementary Table S2). A slight negative Eu anomaly ($\text{Eu}/\text{Eu}^* = 0.70\text{--}0.98$) is present. On the primitive mantle-normalized multi-element diagram, the studied mafic rocks exhibit strong enrichments in Rb, Th, U and Pb and depletions in Nb, Ta, P and Ti (Fig. 4d–f), indicating a typical signature of continental arc basalt^{14,15}.

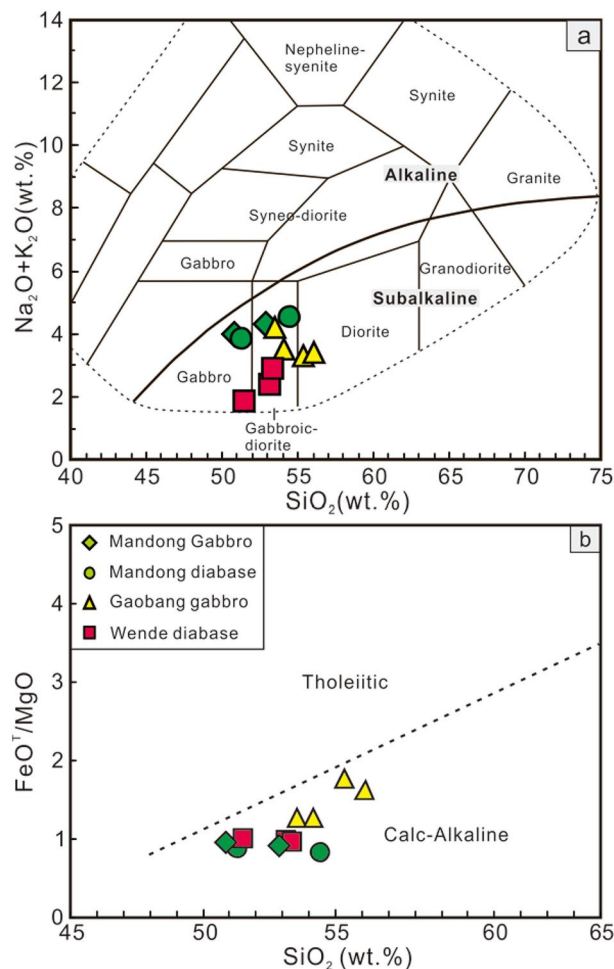


Figure 3. (a) Na₂O + K₂O versus SiO₂ diagram and (b) FeO^T/MgO versus SiO₂ diagram for the Early Cretaceous mafic rocks in the western QHB.

Nd-Hf-O isotopes. Mandong samples have ¹⁴⁷Sm/¹⁴⁴Nd ratios ranging from 0.1275 to 0.1683 and ¹⁴³Nd/¹⁴⁴Nd ratios from 0.51201 to 0.51213, corresponding to $\epsilon_{\text{Nd}}(t)$ values of -9.53 to -11.23 (Fig. 5, Supplementary Table S3). The Wende diabases show relatively lower ¹⁴⁷Sm/¹⁴⁴Nd and ¹⁴³Nd/¹⁴⁴Nd ratios varying from 0.1092 to 0.1116 and 0.51187 to 0.51189, respectively, with lower $\epsilon_{\text{Nd}}(t)$ values of -13.65 to -13.06 (Fig. 5, Supplementary Table S3). Gabbros from Gaobang, however, have the highest ⁴⁷Sm/¹⁴⁴Nd ratios of 0.1324 to 0.1374 and lowest ¹⁴³Nd/¹⁴⁴Nd ratios of 0.51186, corresponding to the lowest $\epsilon_{\text{Nd}}(t)$ values of -14.27 to -14.16 (Supplementary Table S3).

The Mandong and Wende samples have homogenous negative zircon $\epsilon_{\text{Hf}}(t)$ values of -9.45 to -6.17 and -9.39 to -6.36 , respectively (Fig. 6a, Supplementary Table S4). Furthermore, zircon grains from Wende samples have relatively homogenous O isotopic compositions, with $\delta^{18}\text{O}$ values of $+7.03\text{‰}$ to $+7.89\text{‰}$, whereas, those from Mandong samples show variably larger range for zircon $\delta^{18}\text{O}$ values from $+5.72\text{‰}$ to $+8.09\text{‰}$ (Fig. 6b, Supplementary Table S4). The oxygen isotope data in this study are significantly higher than the typical mantle value ($+5.3 \pm 0.3\text{‰}$)¹⁶.

Discussion

New mafic magmatic event in the western Qin-Hang belt of interior South China Block. The mafic rocks in Baotan area from the Northern Guangxi region of the western QHB are traditionally thought to be contemporaneous with widely-exposed Neoproterozoic peraluminous granitoids^{9,11}. Li et al.⁷ reported four mafic dykes that intruded into the Neoproterozoic Sibao Group with ages of 820–830 Ma (mean age 828 ± 7 Ma) by sensitive high-resolution ion microprobe (SHRIMP) zircon U–Pb method. Wang et al.¹¹ conducted LA-ICP-MS zircon U–Pb dating for a layered diabase with an age of 812 ± 5 Ma. Weighted average ²⁰⁶Pb/²³⁸U ages of 855 ± 6 Ma and 835 ± 9 Ma for gabbros were obtained by LA-ICP-MS zircon U–Pb dating by Yao et al.¹⁵ and Chen et al.⁹, respectively. These ages indicate significant mafic magmatism at 855–812 Ma but also led to a widely-accepted assumption that the mafic rocks in the Northern Guangxi of the western QHB are all formed in Neoproterozoic period.

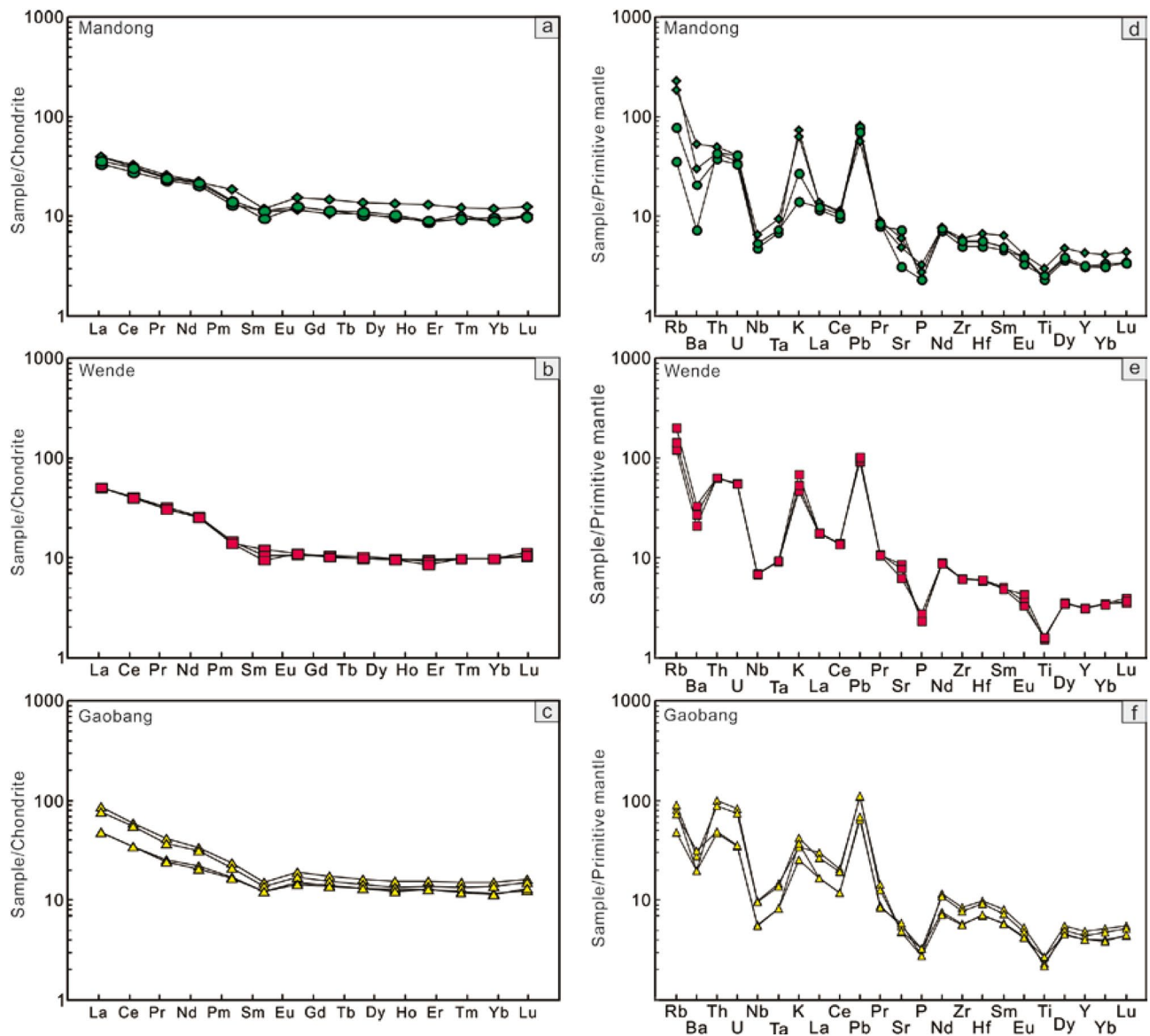


Figure 4. Chondrite-normalized REE patterns (a–c) and primitive mantle normalized multi-element variation diagrams (d–f) of the studied mafic rocks.

During our field work, we noticed some mafic intrusions which are much less weathered than those Neoproterozoic mafic rocks. Three samples from the intrusions were analyzed in different laboratories with different U–Pb dating methods. They gave consistent Early Cretaceous ages ranging from 136 ± 2 Ma to 131 ± 2 Ma (Fig. 2). Thus, we believe that these Early Cretaceous ages are reliable that may reveal a previous undiscovered mafic magmatism event in this region. We noticed that Wang et al.¹⁷ has reported a weighted average age of 100 ± 14 Ma for a lamprophyre in the adjacent region of Baotan in Northern Guangxi. Although this age is also Early Cretaceous, but the accurate data still need to be assessed because only two data points show ages of ~ 100 Ma among 30 analyses¹⁷. Therefore, our data have, for the first time, confirmed the presence of Early Cretaceous mafic rocks in the North Guangxi of the western QHB in spite of their small volume and unclear spatial distribution pattern.

Crustal contamination and fractional crystallization of the mafic magma. Although we observed the presence of some minor secondary minerals in some samples, most of the samples have relatively low loss on ignition (LOI) values of less than 3.0 wt%, and no obvious correlation is shown between the LOI and Nb/La and Th/La ratios, which suggests that the effect of post magmatic alteration is not significant for these studied samples. The petrographic evidence for zircon xenocrysts in the mafic rocks emphasizes the importance of crustal assimilation during magma ascent. In addition, on the $\epsilon_{\text{Nd}}(t)$ versus t diagram (Fig. 5), the studied mafic rocks exhibit negative and variable $\epsilon_{\text{Nd}}(t)$ values of -14.27 to -9.53 and plot in the Proterozoic SCB crust field. The considerable variation of negative $\epsilon_{\text{Nd}}(t)$ values suggests effective contamination of the mafic rocks by crustal materials during magma emplacement. The effect of crustal contamination and assimilation fractionation (AFC) can be evaluated by correlations between major elements (such as MgO, SiO₂ and FeO^T)

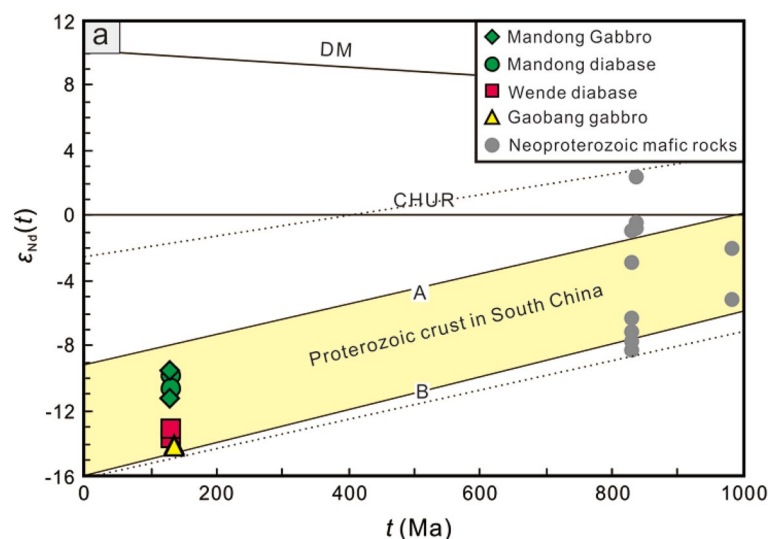


Figure 5. Plots of $\epsilon_{Nd}(t)$ versus t for the studied mafic rocks in the Baotan area.

with trace element ratios (Nb/La, Nb/Th, Th/Ta and Zr/Nb) and isotope compositions^{18–20}. Generally, La/Sm ratios decrease and $\epsilon_{Nd}(t)$ values increase with increasing Nb/La ratios (Fig. 7a,b). In addition, clear positive correlations are found in the bivariate diagrams of Nb/La and $\epsilon_{Nd}(t)$ versus MgO (Fig. 7c,d), similar to AFC trends. These lines of evidence indicate variable crustal contamination during their emplacement en route to the continental crust.

As presented in Fig. 6, the Wende mafic rocks show a relatively limited range of zircon $\epsilon_{Hf}(t)$ values of -9.36 to -6.36 and $\delta^{18}O$ values of $+7.03\text{‰}$ to $+7.89\text{‰}$. Although the Mandong samples exhibit relatively variable $\delta^{18}O$ values from $+5.72\text{‰}$ to $+8.09\text{‰}$ for zircons, they have similar zircon $\epsilon_{Hf}(t)$ values (-9.45 to -6.17) to the Wende samples. Furthermore, no covariation of Hf–O isotopes for the zircon grains from the Mandong and Wende mafic rocks could be observed (Fig. 6c). These facts imply that the effect of an AFC process on the Hf and O isotope composition of the zircon crystals is likely negligible.

Large variations in MgO (4.99–9.81 wt%) and compatible elements such as Cr (125–635 ppm) and Ni (5.98–125 ppm) indicate fractional crystallization of the parental magmas to varying degrees. Cr and Ni decrease sharply and SiO_2 increases with decreasing MgO, showing significant fractionation of olivine and clinopyroxene (Fig. 8a–c). Rapid decreases in FeO^T and TiO_2 with decreasing MgO at $MgO > 7.0$ wt% imply that Fe–Ti oxide were involved in the fractional phase at $MgO > 7.0$ wt% (Fig. 8d,e). The presence of a positive correlation between CaO/Al_2O_3 and CaO demonstrates that plagioclase fractionation is likely (Fig. 8f).

To minimize the effect of assimilation and fractionation crystallization, only the least contaminated and least evolved samples are chosen to constrain the source region. Among the mafic rocks in Baotan area, Mandong gabbros and diabases have the lowest SiO_2 (50.86–54.40 wt%) and highest $\epsilon_{Nd}(t)$ values (-9.53 to -11.23). Their $Mg^\#$ values range from 65 to 68 and therefore these samples are suggested to approximate to the compositions of primary melts.

Magma source. All the mafic rocks in the Baotan area are characterized by relatively high MgO, Cr and Ni (up to 9.81 wt%, 635 ppm and 125 ppm, respectively), suggesting that these rocks originated from a lithospheric mantle source²¹. The crust-like trace element signatures, such as high LREE and large-ion lithophile elements (LILE) contents, low ratios of Nb/Ta (11.57–13.27), Ce/Pb (3.10–5.01) and Nb/U (3.99–5.53), indicate a great contribution of crustal materials in magma sources and/or during subsequent ascending processes^{22–24}. We conducted quantitative modeling to evaluate the contribution of crustal materials based on Nd isotopic compositions by the $(^{143}Nd/^{144}Nd)_i$ -Nd plot (Fig. 9). The compositions of the Neoproterozoic metasedimentary rocks from the Sibao and Danzhou Group are taken as the crustal contaminant^{25,26}. The simple modelling result suggests, that at least 30–45% crustal materials are required in the generation to achieve the observed Nd isotopic compositions of the studied mafic rocks (Fig. 9). However, the assimilation en route of such high-proportional crustal materials is obviously impossible for maintaining the mafic compositions. Moreover, the $\epsilon_{Hf}(t)$ values of the zircon from these mafic rocks are negative and mostly range from -9.47 to -6.17 , whereas their $\delta^{18}O$ values in the range of $+5.72\text{‰}$ to $+8.09\text{‰}$, mostly higher than the mantle value ($+5.3 \pm 0.3\text{‰}$)¹⁶. Thus, these zircon Hf–O isotopes are enriched and coherent with the Nd isotopic compositions of the least contaminated Mandong mafic rock samples. As mentioned above, the AFC process is unlikely responsible for the low $\epsilon_{Hf}(t)$ values and higher $\delta^{18}O$ for the zircon crystals in the mafic rocks. Thus, the observed isotopes abnormalities of the zircons should be ultimately attributed to the composition of their parental magmas. Therefore, the crust-like geochemical signatures, such as high LREE and LILE contents and significant Nb–Ta–Ti negative anomalies, cannot totally be attributed to crustal contamination en route, and probably, are partially inherited from a mantle source modified by subduction-derived components in either recent or ancient metasomatism²⁷.

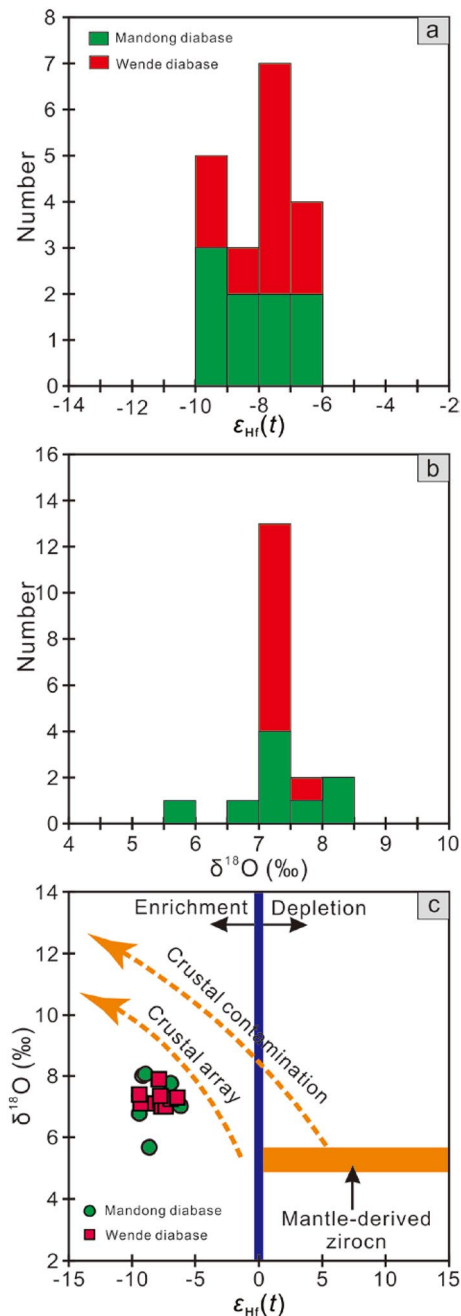


Figure 6. Histogram of Hf–O isotopic data (a,b) and $\epsilon_{\text{Hf}}(t)$ versus $\delta^{18}\text{O}$ correlation diagram (c) of zircon crystals from the studied mafic rocks in the Baotan area.

Subduction is the major mechanism that carries enriched crustal components into mantle source. During the long evolutionary history of the SCB, the lithosphere mantle beneath it experienced several metasomatic events²⁸. Among them, the Neoproterozoic subduction related to the collision between the Yangtze and Cathaysia blocks, or the so-called Jiangnan Orogeny, is the most important²⁹.

In this study, we consider that the Neoproterozoic subduction event is most likely responsible for the crust-like components of the studied mafic rocks. Several lines of evidence support this proposal. Firstly, the antiquity of the metasomatic event would require the metasomatized domain to have remained chemically isolated for a long time, which would have allowed a general isotopic homogenization of the magma source(s)³⁰. Whereas, the absence of isotopic homogenization within the source(s) usually corresponds to a relatively recent metasomatism³⁰. Thus, the Hf isotopic homogeneity in the samples is more consistent with an ancient enrichment event rather than a relatively recent metasomatism in which highly isotopic variability is usually expected to be observed. Furthermore, there is a broad consensus that the Yangtze and Cathaysia blocks, following the northward subduction of an oceanic lithosphere beneath the southeastern Yangtze Block, amalgamated along the Jiangnan Orogen to form a united SCB in the Neoproterozoic time^{31–33}. Subsequently, the SCB turned into an

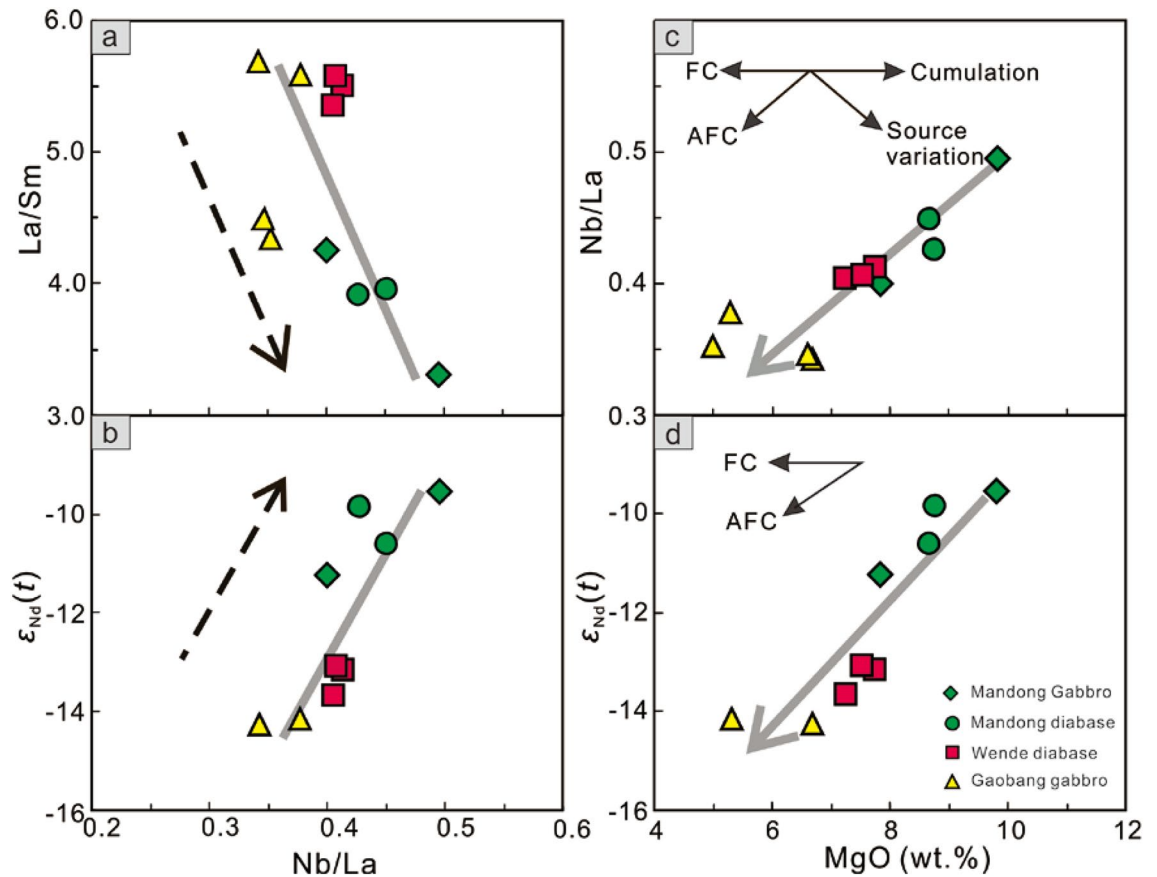


Figure 7. Plots of La/Sm and $\epsilon_{Nd}(t)$ versus Nb/La (a,b), and Nb/La and $\epsilon_{Nd}(t)$ versus MgO (c,d).

intracontinental tectonic development during the latest Neoproterozoic to Cretaceous period^{34–36}. The uniform low $\epsilon_{Hf}(t)$ values with Hf model ages ranging from 1.0 to 1.2 Ga also support a derivation from a Proterozoic metasomatized source. Finally, both the metasedimentary rocks within the Sibao Group and 860–830 Ma mafic rocks intruding into the lower Sibao Group exhibit arc-like geochemical affinity and these rocks were interpreted as the refractory source with addition of crust-derived components by oceanic subduction in an active continental margin setting^{9,31,37}. The regional sedimentary sequences of Sibao and Danzhou Group were deposited at 860–832 and 803–764 Ma and the regional unconformity between them sealed the Jiangnan Orogen and was constrained to be 832–803 Ma, consistent with the presence of 833–822 Ma syn-collisional S-type granites^{15,38}. These data with geological observations indicate the development of the early Neoproterozoic continental arc–basin system along the Jiangnan Orogen. Wang et al.³⁹ and Gan et al.⁴⁰ reported Silurian (ca. 430 Ma) arc-like gabbros and volcanics along the Yunkai–Nanling Domain and Early Jurassic olivine gabbros (ca. 191 Ma) in the Eastern Nanling Range, which have been regarded as derivation of an ancient lithospheric source inherited from the Neoproterozoic metasomatized wedge. When recalculated to 130 Ma, the previously reported Neoproterozoic mafic rocks^{9,41} in the studied areas exhibit $\epsilon_{Nd}(t)$ values of –2.2 to –14.5, covering the ranges of $\epsilon_{Nd}(t)$ values of the investigated mafic rocks in this study (Fig. 5).

Thus, we conclude that, the source for the studied mafic rocks was introduced by the subduction-derived components which is originally with high $\delta^{18}O$ values via the Neoproterozoic subduction process along the western Qin–Hang belt.

Methods

Major, trace element and isotopic analyses. Major and trace element analyses were followed those methods described by Hou et al.⁴² and Qi et al.⁴³, respectively. In brief, we crushed the rock samples to ~200 mesh powder in an agate mill. The analyses were carried out at the National Research Center of GeoAnalysis, Chinese Academy of Geological Sciences, Beijing. Major elements were analyzed by wet chemistry and X-ray fluorescence spectrometry (XRF) with analytical uncertainties ranging from 0.5 to 1.5%. Two standards (granite GSR-1, basalt GSR-3) were used to monitor the analytical quality. Trace elements were determined with a POEMS inductively coupled plasma mass spectrometry (ICP-MS). Analytical uncertainties are 10% for elements with abundances < 10 ppm, and around 5% for those > 10 ppm.

Sm–Nd isotope analyses of whole rock samples followed those procedures described by Chen et al.⁴⁴. The whole rock samples (MD-09, QMS-14, WD-1 and WD-4) were determined by a Finnigan Triton TI thermal ionization mass spectrometer at Tianjin Institute of Geology and Mineral Resources, Tianjin. Procedural blanks yield concentration of < 200 pg for Sm and Nd, and mass fractionation corrections for Nd isotopic ratios were

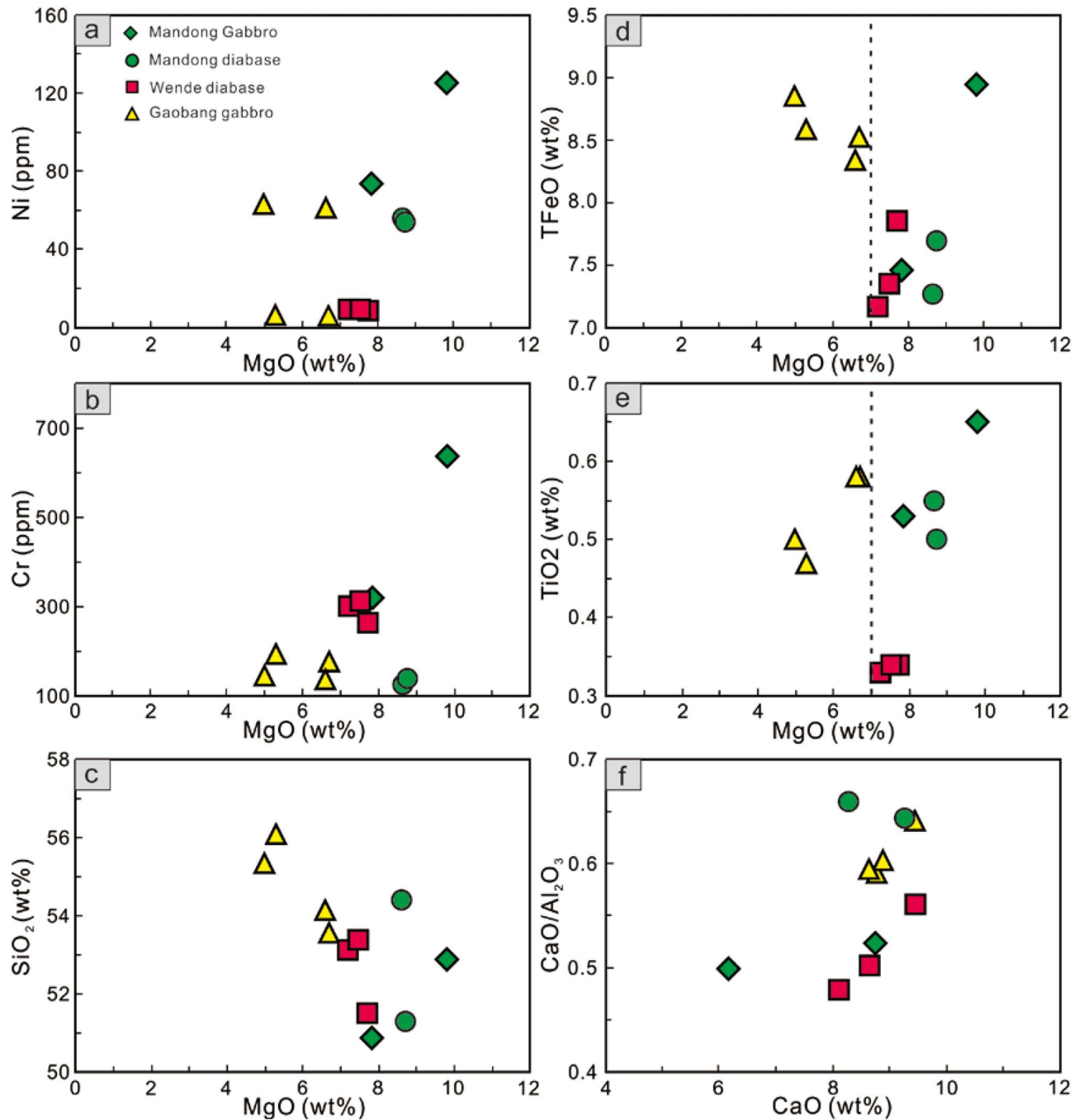


Figure 8. Variation diagrams of Ni, Cr, SiO₂, TFeO and TiO₂ versus MgO (a–e), and CaO/Al₂O₃ versus CaO (f).

based on $^{146}\text{Nd}/^{144}\text{Nd} = 0.7219$. The BCR-2 standard was run regularly and yielded a $^{143}\text{Nd}/^{144}\text{Nd}$ of 0.512642 ± 56 (2σ , $n = 2$). Isotopic analyses of other samples were performed using a Neptune Plus (Thermo Fisher Scientific, MA, USA) multi-collection mass spectrometer equipped with nine Faraday cups and eight ion counters at the Guangzhou Institute of Geochemistry, Chinese Academy of Sciences, Guangzhou. The BHVO-2 standard was run regularly and yielded a $^{143}\text{Nd}/^{144}\text{Nd}$ of 0.512957 ± 47 (2σ , $n = 2$). Measured $^{143}\text{Nd}/^{144}\text{Nd}$ ratios were normalized to $^{146}\text{Nd}/^{144}\text{Nd} = 0.7219$.

Zircon U–Pb dating and Hf–O isotope analysis. Zircon grains were separated from three mafic rocks using standard density and magnetic separation procedures and handpicked under a binocular microscope at the Rock and Minerals Experimental Testing Center of Xinhang Surveying and Mapping Institute, Langfang, Hebei Province. Zircon grains, together with zircon standards Plešovice and Qinghu were mounted together in epoxy discs and then polished to expose the longitudinal section of crystals in half for further analysis. All zircon

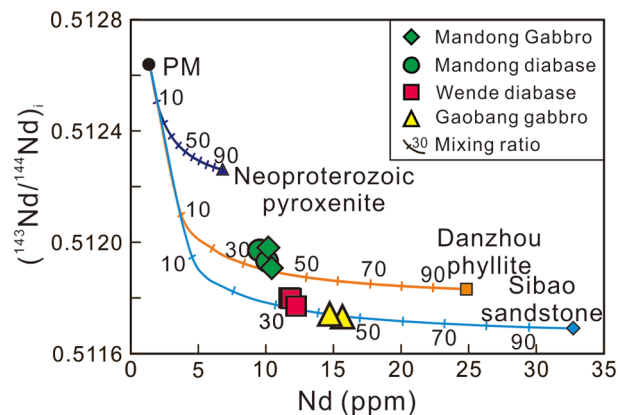


Figure 9. Whole rock $(^{143}\text{Nd}/^{144}\text{Nd})_i$ versus Nd (ppm) diagram showing the modeling results for crustal contamination for the Early Cretaceous mafic rocks.

grains were documented with transmitted and reflected light micrographs as well as CL images to reveal their internal structures. The CL images were performed using the JSM6510 scanning electron microscope attached with a GATAN Chroma CL detector housed at Beijing GeoAnalysis.

Zircon U–Pb dating by SIMS and LA-ICP-MS. Samples from Mandong area (MD-15) and Wende village (WD-1) were vacuum-coated with high purity gold prior to SIMS analysis. Measurements of elements U, Th, and Pb were performed using a Cameca IMS-1280 SIMS at the Institute of Geology and Geophysics, Chinese Academy of Sciences (IGGCAS) in Beijing. The details of the analytical procedures have been described by Li et al.⁴⁵. The O_2^- primary ion beam was accelerated at 13 kV, with an intensity of ca. 10 nA. The resulted ellipsoidal spot is about $20 \times 30 \mu\text{m}$ in size. Positive secondary ions were extracted with a 10 kV potential. In the secondary ion beam optics, a 60 eV energy window was used, together with a mass resolution of ca. 5400 (at 10% peak height), to resolve lead isotopes from isobaric interferences. A single electron multiplier was used in ion-counting mode to measure secondary ion beam intensities by peak jumping mode. Each measurement consists of 7 cycles with the total analytical time of ca. 12 min. U–Th–Pb ratios were determined relative to the standard zircon Plešovice ($^{206}\text{Pb}/^{238}\text{U}$ age of 337 Ma)⁴⁶, and the absolute abundances were calibrated to the 91500 standard zircon (81.2 ppm U and 29 ppm Th)⁴⁷. Pb/U calibration was performed in relation to standard zircon Plešovice and analyses of standards were interspersed with unknown grains. Measured compositions were corrected for common Pb using non-radiogenic ^{204}Pb . An average of present-day crustal composition⁴⁸ is used for the common Pb assuming that it is largely surface contamination introduced during sample preparation. Data reduction was carried out using the Isoplot/Ex v. 3.00 Program⁴⁹. Uncertainties on individual analyses in data tables are reported at 1 sigma level; mean ages for pooled U/Pb analyses are quoted with 95% confidence interval.

U–Pb dating of zircons from Gaobang gabbro (GB2014-1) was performed by LA-ICP-MS at the Key Laboratory of Continental Collision and Plateau Uplift, Institute of Tibetan Plateau Research, Chinese Academy of Sciences in Beijing. A NewWave UP193FX Excimer laser coupled with an Agilent 7500a ICP-MS were used for determination of zircon U–Pb ages and trace element concentrations. The ablation system operated at a wavelength of 193 nm with a spot diameter of 35 μm . Each analysis consists of 15 s background acquisition, 40 s sample data acquisition, and a 45 s washout delay at the end. During the zircon analyses, the standard samples of zircon Plešovice and glass NIST SRM 612 were analyzed first, followed by 8 unknown sample analyses. The standard zircon Plešovice was used for correction of isotope fractionation. Common Pb was corrected following the method proposed by Andersen⁵⁰. U–Pb ages were calculated using the GLITTER 4.0⁵¹ and age plots were carried out using the Isoplot 3.0 program⁴⁹.

Zircon Lu–Hf isotope analysis. In situ Lu–Hf isotopic compositions were measured in previously dated zircon grains at the same domain. Zircon Hf isotope analysis was carried out on a Neptune multi-collector ICP-MS equipped with New Wave UP 213 laser-ablation system at the Institute of Mineral Resources, Chinese Academy of Geological Sciences, Beijing. Instrumental conditions and analytical procedures were comprehensively described by Hou et al.⁵² and a summary is present here. A stationary spot was used for analyses, with a beam diameter of 55 μm . Helium was used as a carrier gas to transport the ablated samples mixed with Argon from the laser-ablation cell to the ICP-MS torch via a mixing chamber. The isobaric interference of ^{176}Lu and ^{176}Yb on ^{176}Hf was corrected using ratios of $^{176}\text{Lu}/^{175}\text{Lu} = 0.02658$ and $^{176}\text{Yb}/^{173}\text{Yb} = 0.796218$ proposed by Chu et al.⁵³. For instrumental mass bias correction, Yb isotope ratios were normalized to $^{172}\text{Yb}/^{173}\text{Yb} = 1.35274$ ⁵³ and Hf isotope ratios to $^{179}\text{Hf}/^{177}\text{Hf} = 0.7325$ using an exponential law⁵⁴. Our routine run of the zircon standard GJ1 gave a weighted mean $^{176}\text{Hf}/^{177}\text{Hf}$ ratio of 0.281979 ± 0.000009 (2σ , $n = 7$), which is in good agreement with the reported value (0.282015 ± 0.000019)⁵⁵.

Zircon oxygen isotope analysis by SIMS. Zircon oxygen isotopes were analyzed using the same Cameca IMS 1280 ion microprobe at IGGCAS, following the analytical procedures of Li et al.⁵⁶. A focused Cs^+ primary ion

beam was accelerated at 10 kV with an intensity of ca. 2 nA. The analyzed spot is ca. 10 μm in diameter. In order to compensate for sample charging, a normal incidence electron flood gun was used with homogeneous electron density over a 100 μm elliptical area. Oxygen isotopes were measured using multi-collection mode on two off-axis Faraday cups (FC). The instrumental mass fractionation (IMF) during the analysis was corrected using the Penglai zircon standard with a $\delta^{18}\text{O}$ value of 5.25‰⁵⁷. Repeated analyzes of an in-house standard Qinghu zircon during the courses of sample analysis yielded mean $\delta^{18}\text{O}$ value of $5.30 \pm 0.23\text{‰}$ (2σ , $n=8$), which is identical within errors to the reported value ($5.39 \pm 0.22\text{‰}$)⁵⁸.

We state that our research did not carry out experiments involving human participants including the use of tissue samples. Our manuscript also did not contain information or images that could lead to identification of a study participant.

Received: 25 December 2020; Accepted: 13 May 2021

Published online: 31 May 2021

References

- Zhang, S. B. & Zheng, Y. F. Formation and evolution of Precambrian continental lithosphere in South China. *Gondwana Res.* **23**, 1241–1260 (2008).
- Li, Z. X. & Li, X. H. Formation of the 1300-km-wide intracontinental orogen and postorogenic magmatic province in Mesozoic South China: A flat-slab subduction model. *Geology* **35**, 179–182 (2007).
- Meng, L. F., Li, Z. X., Chen, H. L., Li, X. H. & Wang, X. C. Geochronological and geochemical results from Mesozoic basalts in southern South China Block support the flat-slab subduction model. *Lithos* **132**, 127–140 (2012).
- Li, X. H. *et al.* Jurassic intraplate magmatism in southern Hunan-eastern Guangxi: $^{40}\text{Ar}/^{39}\text{Ar}$ dating, geochemistry, Sr–Nd isotopes and implications for the tectonic evolution of SE China. *Geol. Soc. Lond. Spec. Publ.* **226**, 193–215 (2002).
- Liu, C. Z., Liu, Z. C., Wu, F. Y. & Chu, Z. Y. Mesozoic accretion of juvenile sub-continental lithospheric mantle beneath South China and its implications: Geochemical and Re–Os isotopic results from Ningyuan mantle xenoliths. *Chem. Geol.* **291**, 186–198 (2012).
- Wang, X. L. *et al.* Detrital zircon geochronology of Precambrian basement sequences in the Jiangnan orogen: Dating the assembly of the Yangtze and Cathaysia Blocks. *Precambrian Res.* **159**, 117–131 (2007).
- Li, Z. X. *et al.* The breakup of Rodinia: Did it start with a mantle plume beneath South China?. *Earth Planet. Sci. Lett.* **173**, 171–181 (1999).
- Wang, X. L. *et al.* LA-ICP-MS U–Pb zircon geochronology of the Neoproterozoic igneous rocks from Northern Guangxi, South China: Implications for tectonic evolution. *Precambrian Res.* **145**, 111–130 (2000).
- Chen, X. *et al.* Contrasting mantle–crust melting processes within orogenic belts: Implications from two episodes of mafic magmatism in the western segment of the Neoproterozoic Jiangnan Orogen in South China. *Precambrian Res.* **309**, 123–137 (2018).
- Li, Z. X. 830–820 Ma mafic to felsic igneous activity in South China and the breakup of Rodinia. *Gondwana Res.* **2**, 591 (1999).
- Wang, X. L. *et al.* LA-ICP-MS U–Pb zircon geochronology of the Neoproterozoic igneous rocks from Northern Guangxi, South China: Implications for tectonic evolution. *Precambrian Res.* **145**, 111–130 (2006).
- Jiang, X. Comparative study of granites geochemical characteristics in North-Northeast Guangxi. *Master thesis*. 1–79 (2019) (in Chinese with English abstract).
- Gou, X. Q. *et al.* LA-ICP-MS zircon U–Pb dating of granite from Longsheng, northern Guangxi. *J. Guilin Univ. Technol.* **40**, 470–479 (2020) (in Chinese with English abstract).
- Kelemen, P. B. *et al.* Reaction between ultramafic rock and fractionating basaltic magma II. Experimental investigation of reaction between olivine tholeiite and harzburgite at 1150–1050 °C and 5 kb. *J. Petrol.* **31**, 99–134 (1990).
- Yao, J. L. *et al.* Neoproterozoic arc-related mafic-ultramafic rocks and syn-collision granite from the western segment of the Jiangnan Orogen, South China: Constraints on the Neoproterozoic assembly of the Yangtze and Cathaysia Blocks. *Precambrian Res.* **243**, 39–62 (2014).
- Valley, J. W. *et al.* Zircon megacrysts from kimberlite: Oxygen isotope variability among mantle melts. *Contrib. Mineral. Petrol.* **133**, 1–11 (1998).
- Wang, L. *et al.* Forming process of lamprophyre from Leidong in Luocheng, Northern Guangxi: Constrains from geochemistry, geochronology and Sr–Nd–Pb isotopes. *Geol. Sci. Technol. Inf.* **34**, 10–19 (2015) (in Chinese with English abstract).
- DePaolo, D. J. Trace element and isotopic effects of combined wall rock assimilation and fractional crystallization. *Earth Planet. Sci. Lett.* **53**, 189–202 (1981).
- Hollanda, M. H. *et al.* Lithosphere–asthenosphere interaction and the origin of Cretaceous tholeiitic magmatism in Northeastern Brazil: Sr–Nd–Pb isotopic evidence. *Lithos* **86**, 34–49 (2006).
- Kozowska, E., Wolska, A., Zuchiewicz, W., Cuong, N. Q. & Pécskay, Z. Crustal contamination of Late Neogene basalts in the Dien Bien Phu Basin, NW Vietnam: Some insights from petrological and geochronological studies. *J. Asian Earth Sci.* **29**, 1–17 (2007).
- Smith, E. I., Sánchez, A., Walker, J. D. & Wang, K. F. Geochemistry of mafic magmas in the hurricane volcanic field, Utah: Implications for small- and large-scale chemical variability of the lithospheric mantle. *J. Geol.* **107**, 433–448 (1999).
- Huppert, H. E., Stephen, R. & Sparks, J. Cooling and contamination of mafic and ultramafic magmas during ascent through continental crust. *Earth Planet. Sci. Lett.* **74**, 371–386 (1985).
- Turner, S. P., Foden, J. D. & Morrison, R. S. Derivation of some A-type magmas by fractionation of basaltic magma: An example from the Padthaway Ridge, South Australia. *Lithos* **28**, 151–179 (1992).
- Gertisser, R. & Keller, J. Temporal variations in magma composition at Merapi Volcano (Central Java, Indonesia): Magmatic cycles during the past 2000 years of explosive activity. *J. Volcano. Geotherm. Res.* **123**, 1–23 (2003).
- Li, X. H. & McCulloch, M. T. Secular variation in the Nd isotopic composition of Neoproterozoic sediments from the southern margin of the Yangtze Block: Evidence for a Proterozoic continental collision in southeast China. *Precambrian Res.* **76**, 67–76 (1996).
- Wang, X. L., Zhou, J. C., Qiu, J. S., Jiang, S. Y. & Shi, Y. R. Geochronology and geochemistry of Neoproterozoic mafic rocks from western Hunan, South China: Implications for petrogenesis and post-orogenic extension. *Geol. Mag.* **145**, 215–233 (2008).
- Smithies, R. H., Van Kranendonk, M. J. & Champion, D. C. The Mesoarchean emergence of modern-style subduction. *Gondwana Res.* **11**, 50–68 (2007).
- Li, S. Z. *et al.* Microplate tectonics: New insights from micro-blocks in the global oceans, continental margins and deep mantle. *Earth Sci. Rev.* **185**, 1029–1064 (2018).
- Zhang, Y. Z., Wang, Y. J., Fan, W. M., Zhang, A. M. & Ma, L. Y. Geochronological and geochemical constraints on the metasomatized source for the Neoproterozoic (~825 Ma) high-Mg volcanic rocks from the Cangshuipu area (Hunan Province) along the Jiangnan domain and their tectonic implications. *Precambrian Res.* **220**, 139–157 (2012).

30. Conticelli, S. *et al.* Trace elements and Sr-Nd-Pb isotopes of K-rich, shoshonitic, and calc-alkaline magmatism of the Western Mediterranean Region: Genesis of ultrapotassic to calc-alkaline magmatic associations in a post-collisional geodynamic setting. *Lithos* **107**, 68–92 (2009).
31. Zhou, J. C., Wang, X. L. & Qiu, J. S. Geochronology of Neoproterozoic mafic rocks and sandstones from northeastern Guizhou, South China: Coeval arc magmatism and sedimentation. *Precambrian Res.* **170**, 27–42 (2009).
32. Yao, J. L., Shu, L. S., Santosh, M. & Li, J. Y. Geochronology and Hf isotope of detrital zircons from Precambrian sequences in the eastern Jiangnan Orogen: Constraining the assembly of Yangtze and Cathaysia Blocks in South China. *J. Asian Earth Sci.* **74**, 225–243 (2013).
33. Wang, X. L. *et al.* Geochemical zonation across a Neoproterozoic orogenic belt: Isotopic evidence from granitoids and metasedimentary rocks of the Jiangnan orogen, China. *Precambrian Res.* **242**, 154–171 (2014).
34. Li, Z. X. *et al.* Magmatic and metamorphic events during the early Paleozoic Wuyi-Yunkai orogeny, southeastern South China: New age constraints and pressure-temperature conditions. *Geol. Soc. Am. Bull.* **122**, 772–793 (2010).
35. Wang, Y. J., Fan, W. M., Zhang, G. W. & Zhang, Y. H. Phanerozoic tectonics of the South China Block: Key observations and controversies. *Gondwana Res.* **23**, 1273–1305 (2013).
36. Wang, Y. J. *et al.* Geochronological, geochemical and Nd-Hf-Os isotopic fingerprinting of an early Neoproterozoic arc-back-arc system in South China and its accretionary assembly along the margin of Rodinia. *Precambrian Res.* **231**, 343–371 (2013).
37. Zhang, Y. Z. & Wang, Y. J. Early Neoproterozoic (~840 Ma) arc magmatism: Geochronological and geochemical constraints on the metabasites in the Central Jiangnan Orogen. *Precambrian Res.* **275**, 1–17 (2016).
38. Su, H. M. *et al.* U–Pb ages and Lu–Hf isotopes of detrital zircons from sedimentary units across the Mid-Neoproterozoic unconformity in the western Jiangnan Orogen of South China and their tectonic implications. *J. Geol.* **126**, 207–228 (2018).
39. Wang, Y. J., Zhang, A. M., Fan, W. M., Zhang, Y. H. & Zhang, Y. Z. Origin of paleosubduction-modified mantle for Silurian gabbro in the Cathaysia Block: Geochronological and geochemical evidence. *Lithos* **160–161**, 37–54 (2013).
40. Gan, C. S., Wang, Y. J., Xin, Q., Bi, M. W. & He, H. Y. Constraints of the Xialan gabbroic intrusion in the Eastern Nanling Range on the Early Jurassic intra-continental extension in eastern South China. *J. Asian Earth Sci.* **145**, 576–590 (2017).
41. Zhou, J. C., Wang, X., Qiu, J. & Gao, J. Geochemistry of Meso- and Neoproterozoic mafic-ultramafic rocks from northern Guangxi, China: Arc or plume magmatism?. *Geochem. J.* **38**, 139–152 (2004).
42. Hou, Z. Q. *et al.* Eocene-Oligocene granitoids in southern Tibet: Constraints on crustal anatexis and tectonic evolution of the Himalayan orogen. *Earth Planet. Sci. Lett.* **349–350**, 38–52 (2012).
43. Qi, L., Hu, J. & Gregoire, D. C. Determination of trace elements in granites by inductively coupled plasma mass spectrometry. *Talanta* **51**, 507–513 (2000).
44. Chen, J. L., Xu, J. F., Wang, B. D., Kang, Z. Q. & Jie, L. Origin of Cenozoic alkaline potassic volcanic rocks at KonglongXiang, Lhasa terrane, Tibetan Plateau: Products of partial melting of a mafic lower-crustal source?. *Chem. Geol.* **273**, 286–299 (2010).
45. Li, X. H., Liu, Y., Li, Q. L., Guo, C. H. & Chamberlain, K. R. Precise determination of Phanerozoic zircon Pb/Pb age by multicollector SIMS without external standardization. *Geochem. Geophys. Geosyst.* **10**, Q04010 (2009).
46. Sláma, J. *et al.* Plešovice zircon—A new natural reference material for U–Pb and Hf isotopic microanalysis. *Chem. Geol.* **249**, 1–35 (2008).
47. Wiedenbeck, M. *et al.* Three natural zircon standards for U–Th–Pb, Lu–Hf, trace-element and REE analyses. *Geostandard Newslett.* **19**, 1–23 (1995).
48. Stacey, J. S. & Kramers, J. D. Approximation of terrestrial lead isotope evolution by a two-stage model. *Earth Planet. Sci. Lett.* **26**, 207–221 (1975).
49. Ludwig, K. R. User's Manual for Isoplot/Ex version 3.00—A geochronology toolkit for microsoft excel. *Berkeley Geochronol. Center Spec. Publ.* **4**, 1–70 (2003).
50. Andersen, T. Correction of common Pb in U–Pb analyses that do not report ²⁰⁴Pb. *Chem. Geol.* **192**, 59–79 (2002).
51. Jackson, S. E., Pearson, N. J., Griffin, W. L. & Belousova, E. A. The application of laser ablation-inductively coupled plasma-mass spectrometry to in situ U–Pb zircon geochronology. *Chem. Geol.* **211**, 47–69 (2004).
52. Hou, K. J. *et al.* Laser ablation-MC-ICP-MS technique for Hf isotope microanalysis of zircon and its geological applications. *Acta Petrol. Sin.* **23**, 2595–2604 (2007) (in Chinese with English abstract).
53. Chu, N. C. *et al.* Hf isotope ratio analysis using multi-collector inductively coupled plasma mass spectrometry: An evaluation of isobaric interference corrections. *J. Anal. At. Spectrom.* **17**, 1567–1574 (2002).
54. Wu, F. Y., Yang, Y. H., Xie, L. W., Yang, J. H. & Xu, P. Hf isotopic compositions of the standard zircons and baddeleyites used in U–Pb geochronology. *Chem. Geol.* **234**, 105–126 (2006).
55. Elhlou, S., Belousova, E., Griffin, W., Pearson, N. & O'Reilly, S. Trace element and isotopic composition of GJ-red zircon standard by laser ablation. *Geochim. Cosmochim. Acta* **70**, A158 (2006).
56. Li, X. H. *et al.* Role of mantle-derived magma in genesis of early Yanshanian granites in the Nanling Range, South China: In situ zircon Hf–O isotopic constraints. *Sci. China Ser. D Earth Sci.* **52**, 1262–1278 (2009).
57. Li, X. H. *et al.* Penglai zircon megacrysts: A potential new working reference for microbeam analysis of Hf–O isotopes and U–Pb age. *Geostand. Geoanal. Res.* **34**, 117–134 (2010).
58. Li, X. H. *et al.* Qinghu zircon: A working reference for microbeam analysis of U–Pb age and Hf and O isotopes. *Chin. Sci. Bull.* **58**, 4647–4654 (2013).

Acknowledgements

This research was financially supported by the National Natural Science Foundation of China (41873041) and the MOST Special Fund from the State Key Laboratory of Geological Processes and Mineral Resources, China University of Geosciences (No. MSFGPMR03-2). Jin-Huo Wang is thanked for his help during the field sampling and discussion during the preparation of this manuscript. Comments and suggestions from Prof. Xiaolei Wang and two reviewers improved this manuscript significantly.

Author contributions

S.Y.J. and H.M.S. conceived the idea. H.M.S., J.B.S. and D.Y.Z. collected the samples and performed analyses. X.K.W. and X.Q.H. joined the field work. H.M.S. and S.Y. J. interpreted the data and wrote the manuscript. All authors reviewed the manuscript before the submission.

Competing interests

The authors declare no competing interests.

Additional information

Supplementary Information The online version contains supplementary material available at <https://doi.org/10.1038/s41598-021-91045-1>.

Correspondence and requests for materials should be addressed to S.-Y.J.

Reprints and permissions information is available at www.nature.com/reprints.

Publisher's note Springer Nature remains neutral with regard to jurisdictional claims in published maps and institutional affiliations.



Open Access This article is licensed under a Creative Commons Attribution 4.0 International License, which permits use, sharing, adaptation, distribution and reproduction in any medium or format, as long as you give appropriate credit to the original author(s) and the source, provide a link to the Creative Commons licence, and indicate if changes were made. The images or other third party material in this article are included in the article's Creative Commons licence, unless indicated otherwise in a credit line to the material. If material is not included in the article's Creative Commons licence and your intended use is not permitted by statutory regulation or exceeds the permitted use, you will need to obtain permission directly from the copyright holder. To view a copy of this licence, visit <http://creativecommons.org/licenses/by/4.0/>.

© The Author(s) 2021